THE JOURNAL OF PHYSICAL CHEMISTRY Letters

Letter

pubs.acs.org/JPCL

Proton Transfer of Guanine Radical Cations Studied by Time-Resolved Resonance Raman Spectroscopy Combined with Pulse Radiolysis

Jungkweon Choi,[*,†,‡] Cheolhee Yang,[‡,§] Mamoru Fujitsuka,[†] Sachiko Tojo,[†] Hyocherl Ihee,[‡,§] and Tetsuro Majima[*,†]

[†]The Institute of Scientific and Industrial Research (SANKEN), Osaka University, Mihogaoka 8-1, Ibaraki, Osaka 567-0047, Japan

[‡]Center for Nanomaterials and Chemical Reactions, Institute for Basic Science (IBS), Daejeon 305-701, Republic of Korea

[§]Department of Chemistry, Korea Advanced Institute of Science and Technology (KAIST), Daejeon 305-701, Republic of Korea

Supporting Information

ABSTRACT: The oxidation of guanine (G) is studied by using transient absorption and time-resolved resonance Raman spectroscopies combined with pulse radiolysis. The transient absorption spectral change demonstrates that the neutral radical of G ($G^{\bullet}(-H^{+})$), generated by the deprotonation of G radical cation ($G^{\bullet+}$), is rapidly converted to other G radical species. The formation of this species shows the pH dependence, suggesting that it is the G radical cation $(G^{\bullet+})'$ formed from the protonation at the N7 of $G^{\bullet}(-H^{+})$. On one hand, most Raman bands of $(G^{\bullet+})'$ are up-shifted relative to those of G, indicating the increase in the bonding order of pyrimidine (Pyr) and imidazole rings. The $(G^{\bullet+})'$ exhibits the characteristic CO stretching mode at ~1266 cm^{-1} corresponding to a C−O single bond, indicating that the unpaired electron in $(G^{\bullet+})'$ is localized on the oxygen of the Pyr ring.

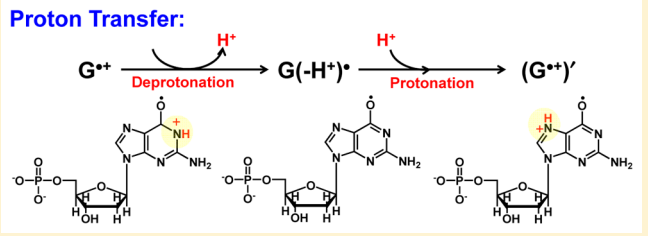

DNA damages induced by metabolic or hydrolytic processes lead to the DNA mutation and a variety of fatal diseases.[1] Among DNA damages, oxidative DNA damage occurs most frequently in cells and is caused by the reactive oxygen species (ROS), which are generated from normal cellular metabolism.[2−8] Thus, the oxidative DNA damage is considered to be an inevitable cellular process. Furthermore, ROS are also produced by exogenous sources such as ionizing or ultraviolet (UV) radiation and carcinogenic compounds. Meanwhile, the reduction of DNA sequence is related to the DNA repair process. For example, cyclobutane pyrimidine dimers (CPD),[9,10] which are major DNA lesions induced by UV radiation, can be repaired by one electron transfer from photosensitizers to the CPD lesion.[11−14] From these points of view, the redox reactions in the DNA strand have been experimentally and theoretically investigated in the biochemical and biomedical field in terms of the DNA damage and the repair of damaged DNA.

It is well-known that the oxidative DNA damage is initiated by radical cations of nucleic acid bases formed by the reaction between nucleic acid bases and ROS.[7,8] Therefore, the characterization of structures and reactivities of radical cations of four nucleotides is crucial for understanding DNA damage and repair processes. Furthermore, the proton transfer occurring in aqueous solution containing four nucleotides is coupled to numerous biological reactions. In this respect, numerous theoretical and experimental studies have been exclusively focused on the oxidation of guanine (G), because G with the lowest oxidation potential among four nucleotides (A, T, G, and C) is easily oxidized to G radical cation, $G^{\bullet+}$.[15−18] Moreover, it has been suggested that $G^{\bullet+}$ in aqueous solution quickly converts to the neutral radical ($G^{\bullet}(-H^{+})$) through the loss of imino proton N1−H (deprotonation) (see Scheme 1).[19−24] However, the structure and reactivity of $G^{\bullet+}$ and $G^{\bullet}(-H^{+})$ are still unclear. Indeed, various structures for $G^{\bullet+}$ and $G^{\bullet}(-H^{+})$ have been suggested, as depicted in Figure S1. The ESR experiment conducted by Rakvin et al. demonstrated that in 2′-deoxyguanosine-5′-monophosphate (5′-dGMP), $G^{\bullet+}$ generated during the γ-irradiation at 4.2 K shows the large spin density at the oxygen of the Pyr ring (C6−O).[19] Meanwhile, some research groups suggested that the spin density in $G^{\bullet+}$ is localized mainly on the N3, C5, N7, or C8-sites.[25−28] In addition, the proton transfer and reactivity of $G^{\bullet+}$ generated from oxidation of G are still matters of debate.[27−31] To address these issues, we have investigated the structure and reactivity of $G^{\bullet+}$ and $G^{\bullet}(-H^{+})$ by using time-resolved resonance Raman (TR^{3}) and ultraviolet−visible (UV−vis) absorption spectroscopies combined with pulse radiolysis. Because pulse radiolysis can selectively and efficiently generate radical ions during the irradiation with high-energy electrons, this method has been used extensively to study the reactivity of radical ions generated from the redox reactions of various molecules.[32−37] On the

Received: October 16, 2015
Accepted: December 3, 2015
Published: December 3, 2015

DOI: 10.1021/acs.jpclett.5b02313
J. Phys. Chem. Lett. 2015, 6, 5045−5050

Scheme 1. Representative Oxidation of Guanine (G) and the Deprotonation of $G^{\bullet+}$

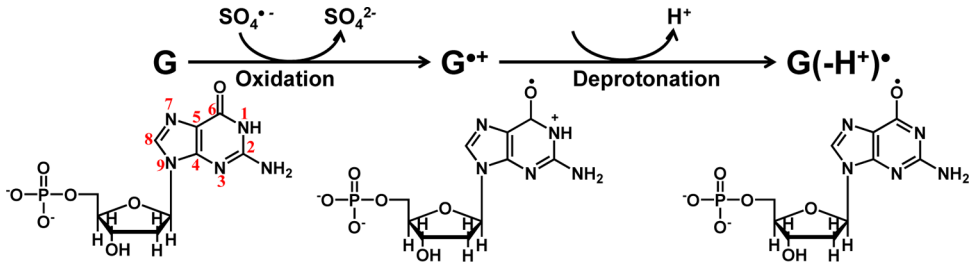

other hand, TR^3 spectroscopy is a powerful technique for elucidating the structures of radical ions generated during pulse radiolysis in a vibrational level.[38−40] In the present study, we clearly observed for the first time the protonation of $G^{\bullet}(-H^+)$ occurring with a rate constant of 8.1×10^6 s^{-1}: $G^{\bullet}(-H^+) + H^+ \rightarrow (G^{\bullet+})'$. Furthermore, Raman signals of G radical ions generated during pulse radiolysis are reported for the first time, to the best of our knowledge, and we discuss the structures and reactivities of $G^{\bullet+}$ and $G^{\bullet}(-H^+)$ based on the results obtained from transient absorption and TR^3 experiments.

To study the structure and reactivity of $G^{\bullet+}$ generated during the pulse radiolysis, we used 2′-deoxyguanosine-5′-monophosphate (5′-dGMP). The $G^{\bullet+}$ can be easily formed by the oxidation of G using pulse radiolysis. The hydrated electron (e_{aq}^-) generated during pulse radiolysis in aqueous solution containing ammonium persulfate ($(NH_4)_2S_2O_8$) and *tert*-butyl alcohol (as the scavenger of OH radicals) quickly reacts with a peroxydisulfate ($S_2O_8^{2-}$) to produce sulfate radical anion ($SO_4^{\bullet-}$), which is a strong oxidant (eq 1).[41,42] Then, G is oxidized to $G^{\bullet+}$ by $SO_4^{\bullet-}$ (eq 2).[41]

$$e_{aq}^- + S_2O_8^{2-} \rightarrow SO_4^{2-} + SO_4^{\bullet-} \quad (1)$$

$$SO_4^{\bullet-} + G \rightarrow SO_4^{2-} + G^{\bullet+} \quad (k = 4.6 \times 10^9\ M^{-1}\ s^{-1}) \quad (2)$$

Figure 1a shows the transient absorption spectra observed at various times after an 8 ns electron pulse during pulse radiolysis of 50 mM 5′-dGMP in 100 mM Na phosphate buffer (pH 7.4) containing 0.1 M ammonium persulfate ($(NH_4)_2S_2O_8$) and 0.1 M *tert*-butyl alcohol. As shown in Figure 1a, the absorption spectrum observed at Δt = 30 ns has two absorption bands with maxima located around 380 and 520 nm. The absorption signal around 380 nm increased at short delay times (Δt = 30−300 ns) and then decreased in the long delay time (>1 μs), whereas the broad signal around 520 nm concomitantly decreases with a blue-shift as increasing the delay time. The time profile of the transient absorption at 400 nm shows the fast rising and slow decay features, while the time profile measured at 570 nm exhibits the fast and slow decay features (see the inset in Figure 1a). Both time profiles measured at 400 and 570 nm were well reproduced by a biexponential function, as shown in Figure 1a. The rate constant for the rise component observed at 400 nm is close to that for the fast decay component observed at 570 nm. Therefore, two time profiles measured at 400 and 570 nm are analyzed by the global fitting using a biexponential function. From the global fitting analysis, the rate constant for the rise component observed at 400 nm is determined to be $8.1 \pm 0.2 \times 10^6$ s^{-1} (~123 ns) (see Figure S2).

The absorption spectrum observed at Δt = 30 ns is similar to that of $G^{\bullet}(-H^+)$ assigned by Candeias and Steenken,[41] implying that the absorption spectrum observed at Δt = 30 ns may be attributed to $G^{\bullet}(-H^+)$ and the $G^{\bullet+}$ converts to the $G^{\bullet}(-H^+)$ within 30 ns. Considering the rate constant on the formation of $G^{\bullet+}$ (4.6×10^9 M^{-1} s^{-1}) and the concentration of 5′dGMP (50 mM), the $G^{\bullet+}$ under experimental conditions is formed within the laser pulse width (<7 ns). In addition, Stemp et al. suggested that the loss of imino proton at N1 takes place within 50 ns.[43] Kobayashi et al. also revealed that in the case of free G base (5′-dGMP), the imino proton N1−H is released into solvent with a rate constant of 1.8×10^7 s^{-1} (~56 ns) at pH 7.0 because of the low pK_a value of N1−H (pK_a 3.9) of

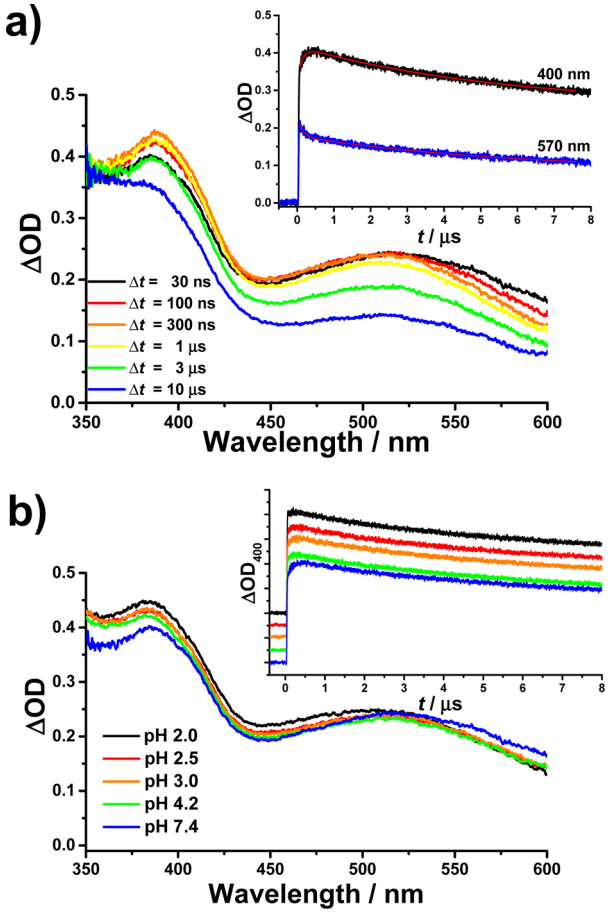

Figure 1. (a) Transient absorption spectra observed at various times after an 8 ns electron pulse during pulse radiolysis of 5′-dGMP in 100 mM Na phosphate buffer (pH 7.4) containing 0.1 M ammonium persulfate ($(NH_4)_2S_2O_8$) and 0.1 M *tert*-butyl alcohol. The inset shows the decay profiles monitored at 400 and 579 nm. (b) Transient absorption spectra observed at 30 ns after an 8 ns electron pulse during pulse radiolysis of 5′-dGMP as a function of the pH value. The inset shows the decay profiles monitored at 400 nm in solutions with various pH values.

DOI: 10.1021/acs.jpclett.5b02313
J. Phys. Chem. Lett. 2015, 6, 5045−5050

$G^{\bullet+}$.[20] These previous results are consistent with our result and support the fact that the absorption spectrum observed at Δt = 30 ns is attributed to $G^{\bullet}(-H^{+})$, which is formed by the deprotonation of $G^{\bullet+}$ occurring within 30 ns. On one hand, the deprotonation rate of $G^{\bullet+}$ determined in the present study is much faster than those observed from various DNA strands. In dsDNA with a G−C base pair formed by hydrogen bonding, the imino proton N1−H of $G^{\bullet+}$ is transferred to N3 of cytosine (C) with a rate constant of (3.3−3.6) × 10^6 s^{-1} at pH 7.0.[20] In contrast to free G base and dsDNA, Wu et al. demonstrated that the deprotonation of $G^{\bullet+}$ generated from G-quadruplex occurs at N2−H with a rate constant of 2.1× 10^5 s^{-1} at pH 7.0.[44] It is known that in both dsDNA and G-quadruplex, the deprotonation process from $G^{\bullet+}$ to $G^{\bullet}(-H^{+})$ leads to the red-shift in the absorption band around 520 nm.[20,45] However, the fast dynamics of 8.1 × 10^6 s^{-1} observed in the present study leads to the blue-shift in the transient absorption band, as depicted in Figure 1a. Therefore, we conclude that the absorption spectra observed at Δt = 30 ns is attributed to $G^{\bullet}(-H^{+})$ and that the process with the rate constant of 8.1 × 10^6 s^{-1} is not due to the deprotonation process of $G^{\bullet+}$ but is attributed to an unknown reaction of $G^{\bullet}(-H^{+})$.

To further elucidate the process with the rate constant of 8.1 × 10^6 s^{-1}, the pH dependence on the oxidation of G was investigated by a transient absorption measurement using pulse radiolysis. When the pH value decreased, the absorption signal around 380 nm increased, as shown in Figure 1b, whereas the broad signal around 520 nm is slightly blue-shifted. The rising feature in the time profile measured at 400 nm gradually disappeared with decreasing pH value. Notably, as depicted in Figure 2, the rate constant for the rise component increases

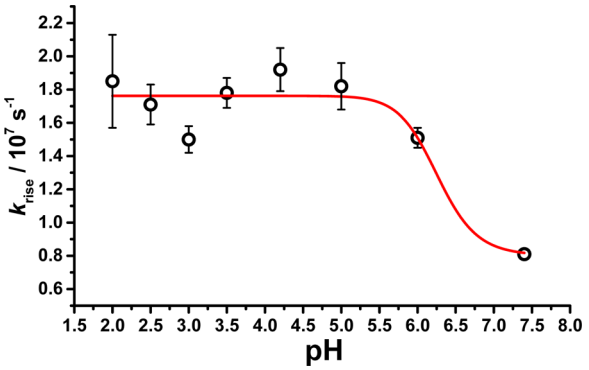

Figure 2. pH dependence on the rate constants determined from the rise component of the decay profiles measured at 400 nm.

with decreasing pH value and then shows the constant values in the low pH solutions (pH <5.0), indicating that the fast dynamics observed in the present study is dependent on the pH of the solution. Generally, the deprotonation process in solution with a pH lower than the pK_a value should slowly occur because of the higher proton concentration. Consequently, the rate constant for the deprotonation process should decrease with the decrease of the pH value. However, as shown in Figure 2, the opposite result was observed. That is, the rate constant for the fast dynamics increased with decreasing pH value. This result indicates that the fast dynamics is not due to the deprotonation process but is probably due to the protonation of $G^{\bullet}(-H^{+})$, leading to the formation of other G radical species ($(G^{\bullet+})'$; $G^{\bullet}(-H^{+}) + H^{+} \rightarrow (G^{\bullet+})'$). Thus, the slower decay component with a long lifetime is attributed to $(G^{\bullet+})'$. The protonation of $G^{\bullet}(-H^{+})$ to $(G^{\bullet+})'$ will be further discussed later.

To clarify the structures of $G^{\bullet+}$, $G^{\bullet}(-H^{+})$, and $(G^{\bullet+})'$, we measured the TR^3 spectra of 50 mM 5′-dGMP in 100 mM Na phosphate buffer (pH 7.4) by using a 532 nm laser pluse. Figure 3 shows the TR^3 spectra observed at various times after

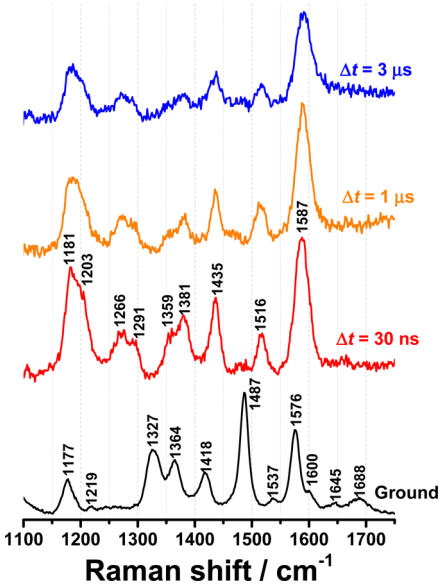

Figure 3. TR^3 spectra observed at various times after an 8 ns electron pulse during pulse radiolysis of 50 mM 5′-dGMP in 100 mM Na phosphate buffer (pH 7.4; λ_{Ex} = 532 nm).

an 8 ns electron pulse during pulse radiolysis of 5′-dGMP in 100 mM Na phosphate buffer containing 0.1 M ammonium persulfate ($(NH_4)_2S_2O_8$) and 0.1 M *tert*-butyl alcohol. Based on the assignments of resonance Raman spectra of 5′-dGMP, as reported by Toyama et al.[46] and Fodor et al.,[47] Raman bands of 5′-dGMP (G) in 100 mM Na phosphate buffer are assigned and listed in Table 1. In the case of 5′-dGMP, the more intensive peaks appear at 1327, 1487, and 1576 cm^{-1}, which are attributed to the Im (N7) ring stretching, Pyr ring CN stretching coupled with 8-CH deformation, and Pyr (N3) ring stretching, respectively. The Raman band due to C6═O stretching is observed at 1688 cm^{-1}. It is worth noting that, as shown in Figure 3, the TR^3 spectra measured at various times after an 8 ns electron pulse during pulse radiolysis of 5′-dGMP are very similar. This is unexpected because the protonation of $G^{\bullet}(-H^{+})$ with a rate constant of 8.1 × 10^6 s^{-1} should bring about the difference between TR^3 spectra measured at Δt = 30 ns and ≥1 μs. However, the experimental results clearly showed that the TR^3 spectra are independent of the delay time, although the intensities of Raman bands are slightly decreased with increasing delay time. The similarity in TR^3 spectra measured at 30 ns and ≥1 μs implies that all TR^3 spectra measured at various delay times after an 8 ns electron pulse are attributed to the same transient species. Considering the lifetime of each G radical species obtained by transient absorption experiments, the observed TR^3 spectra are originated probably from $(G^{\bullet+})'$. One cannot rule out the possibility that Raman bands for $G^{\bullet}(-H^{+})$ are not affected by the protonation. However, this possibility is in contrast to the fact that the protonation of a chemical species can significantly affect its molecular geometry and Raman band. Therefore, we

DOI: 10.1021/acs.jpclett.5b02313
J. Phys. Chem. Lett. 2015, 6, 5045−5050

Table 1. Raman Bands Observed for 5′-dGMP and $(G^{\bullet+})'$ in 100 mM Na Phosphate Buffer (pH 7.4) Containing 0.1 M Ammonium Persulfate ($(NH_4)_2S_2O_8$) and 0.1 M *tert*-Butyl Alcohol

assignment of Raman bands	5′-dGMP (cm^{-1})	$(G^{\bullet+})'$ (cm^{-1})
Pyr(N3) pyrimidine ring mode localized at N_3	1177	1181
Im(C8−N9) vibration mode localized at the C8−N9 linkage	1219	–
C−O single bond	–	1266
Im(N7) Vibration localized within the imidazole ring	1327	1359
C2═N3−C4−N9 stretch; stretch mode of the C_2═N_3−C_4−N_9 moiety	1364	1381
Pyr + Im vibration involving both the pyrimidine and imidazole ring	1418	1435
Pyr ring CN stretch + 8-CH def	1487	1516
Pyr + Im vibration delocalized over the pyrimidine and imidazole ring	1537	–
Pyr(N3) pyrimidine ring mode contributed largely from a motion of N_3	1576	1587
Pyr(C2) + N1−H bend pyrimidine ring mode largely localized at C_2 and weakly coupled with the N_1−H bend	1600	–
C2−NH2 scissors	1645	–
C6═O stretch	1688	–

suggest that the TR^3 spectra observed at various times after an 8 ns electron pulse during pulse radiolysis of G are dominantly attributed to $(G^{\bullet+})'$ rather than $G^{\bullet}(-H^+)$, suggesting that the vibrational modes of $(G^{\bullet+})'$ are more Raman active than those of $G^{\bullet}(-H^+)$.

The TR^3 spectrum of $(G^{\bullet+})'$, shown in Figure 3, is significantly different from that of G. Most Raman bands measured for $(G^{\bullet+})'$ are up-shifted relative to those of G. In particular, the largest shifts were observed for TR^3 bands at 1359 and 1516 cm^{-1}, corresponding to Im (N7) and Pyr ring CN stretching coupled with 8-CH deformation, respectively. The observed up-shifts imply that the whole bond strengths of Pyr and Im rings for $(G^{\bullet+})'$ are relatively larger than those for G. In the TR^3 bands of $(G^{\bullet+})'$, the most prominent peak is observed at 1266 cm^{-1}. It is noteworthy that the Raman band at 1688 cm^{-1} corresponding to C6═O stretching observed for G disappears upon the oxidation, followed by the appearance of a new Raman band at 1266 cm^{-1}. The absence of the C6═O stretching mode at >1600 cm^{-1} in $(G^{\bullet+})'$ means the decrease of the C═O double-bond character. In other words, this result implies that the unpaired electron in $(G^{\bullet+})'$ is localized on the oxygen of the Pyr ring or is delocalized on the Pyr ring, consequently leading to the decrease of the C═O double-bond order. Based on this result, two structures for $(G^{\bullet+})'$ shown in Scheme 2 can be expected: one is $(G^{\bullet+})'$-I with a C−O single bond due to an unpaired electron localized on the oxygen of the Pyr ring, and the other is $(G^{\bullet+})'$-II with a partial C⋯O double bond formed by an unpaired electron delocalized on the Pyr ring. Generally, it has been accepted that in phenoxyl radical, the Raman bands corresponding to a C−O single bond and a partial C⋯O double bond appear at ∼1250 and ∼1510 cm^{-1}, respectively.[48−52] Thus, we suggest that the Raman band at 1266 cm^{-1} is originated from a C−O single bond for $(G^{\bullet+})'$, although the 1266 cm^{-1} frequency is slightly higher than that of a C−O single bond measured from phenoxyl radical. On the other hand, one cannot rule out the possibility that the Raman band at 1516 cm^{-1} is attributed to a partial C⋯O double-bond stretching of $(G^{\bullet+})'$-II formed by an unpaired electron delocalized on the Pyr ring. The delocalization of an unpaired electron on the Pyr ring upon oxidation induces the decrease of the bond strength in the Pyr ring, resulting in the down-shift of Raman bands related to the Pyr ring. However, as mentioned above, most of Raman bands measured for $(G^{\bullet+})'$ are slightly up-shifted compared to those for G. This result indicates that the Raman band at 1516 cm^{-1} is attributed to the Pyr ring CN stretching coupled with 8-CH deformation, but not a partial C⋯O double-bond stretching. Therefore, we suggest that $(G^{\bullet+})'$ exists dominantly as a $(G^{\bullet+})'$-I with a C−O single bond. Candeias and Steenken suggested that the unpaired electron in $(G^{\bullet+})'$ resides mainly on the oxygen of the Pyr ring (C6−O), although various tautomers due to the high aromaticity coexist in aqueous solutions.[41] Rakvin et al. also demonstrated that the large spin density in $G^{\bullet+}$ was observed at the O6-site.[19] These previous results imply that the unpaired electron may be localized on the oxygen of the Pyr ring and support our suggestion that the unpaired electron in $(G^{\bullet+})'$ is localized on the oxygen of the Pyr ring. Furthermore, we also suggest that the unpaired electron in $G^{\bullet+}$ and $G^{\bullet}(-H^+)$ is localized on the oxygen of the Pyr ring, but not on the N3, C5, N7, or C8 sites.

On the basis of the results obtained in the present study, we consider the proton transfer between $G^{\bullet}(-H^+)$ and the water molecule, especially the protonation process of $G^{\bullet}(-H^+)$, $(G^{\bullet}(-H^+) + H^+ \rightarrow (G^{\bullet+})')$. It is well-known that the pK_a of N1 in $G^{\bullet+}$ is 3.9.[20,41] In addition, our experimental result demonstrates that the deprotonation at N1 of $G^{\bullet+}$ rapidly occurs within 30 ns. Stemp et al. also suggested that the loss of imino proton at N1 takes place within 50 ns.[43] Considering the deprotonation rate ($k_d > 3.3 \times 10^7$ s^{-1}), the pK_a of 3.9, and the pH value of the solution (pH ∼7), the protonation rate constant k_p at N1 can be estimated to be about $\geq 2.6 \times 10^4$ s^{-1} under the experimental conditions. The small value for k_p implies that the reprotonation at N1 takes place in the time range of the microsecond. From this point of view, in $G^{\bullet}(-H^+)$, N3 and N7 can be considered as a protonation site, but not N1. Giese and McNaughton demonstrated that the proton affinity for protonation at N7 of G is calculated to be 945 kJ mol^{-1},[53] which is close to that reported by Greco et al. (951 ± 48 kJ mol^{-1}).[54] Giese and McNaughton also suggested that N7, and not N3, is the preferred protonation site in both aqueous solution and solid states. Steenken suggested that $G^{\bullet+}$ in the neutral solutions is in equilibrium with $(G^{\bullet+})'$ (see Scheme II in ref 55).[55] Tomasz et al. proposed that the isotope exchange at the C8-site of the Im ring requires the protonation at N7 as a first step at various pH values at 37 °C,[56] meaning that the N7 of the Im ring can be easily protonated under the physiological conditions. Therefore, we suggest that the fast dynamics observed in the transient absorption measurement is due to the protonation at N7 of $G^{\bullet}(-H^+)$. As mentioned above, the protonation at N7 of $G^{\bullet}(-H^+)$ may greatly affect the molecular geometry of the Im ring, resulting in the large shift of a Raman band. Among Raman bands for $G^{\bullet}(-H^+)$, indeed, the

Scheme 2. Structures of $(G^{\bullet+})'$

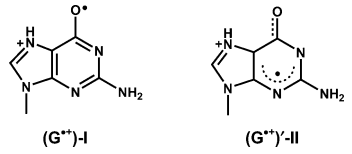

$(G^{\bullet+})$-I $(G^{\bullet+})'$-II

DOI: 10.1021/acs.jpclett.5b02313
J. Phys. Chem. Lett. 2015, 6, 5045−5050

largest upshift was observed for vibration within the Im (N7) ring, supporting that the protonation site in $G^{\bullet}(-H^{+})$ is the N7, but not N3. The plot of the rate constant against the pH value (Figure 2) demonstrates that the pK_a of N7 in $G^{\bullet}(-H^{+})$ may be higher than 6.0. This means that the $G^{\bullet}(-H^{+})$ can be easily converted to $(G^{\bullet+})'$ under the physiological conditions.

In conclusion, we have studied the oxidation of G, which has the lowest oxidation potential among four nucleotides (A, T, G, and C), by using the transient absorption and TR^3 spectroscopies combined with pulse radiolysis. Although the redox reaction in the DNA strand has been extensively investigated in the fields of biomedical science and nanobiotechnology, the proton transfer of radical cations of four nucleotides are still unclear. The results presented herein show that the $G^{\bullet+}$ formed by one-electron oxidation rapidly releases the imino proton N1−H into water within an 8 ns electron pulse, resulting in the formation of $G^{\bullet}(-H^{+})$. In addition, the $G^{\bullet}(-H^{+})$ is converted to another G protonated radical cation ($(G^{\bullet+})'$) with a rate constant of 8.1×10^6 s^{-1}: $G^{\bullet}(-H^{+}) + H^{+} \rightarrow (G^{\bullet+})'$. In $G^{\bullet}(-H^{+})$, N7 is considered as a protonation site, but not N1 and N3.

In addition, Raman signals of G radical ions generated upon pulse radiolysis were measured, for the first time, in the present study. The TR^3 bands for 5′-dGMP are assigned to those of $(G^{\bullet+})'$. The $(G^{\bullet+})'$ exhibited the characteristic CO stretching mode at ∼1266 cm^{-1} corresponding to a C−O single bond. The result presented herein demonstrates that $(G^{\bullet+})'$ exists as $(G^{\bullet+})'$-I with a C−O single bond due to an unpaired electron localized on the oxygen of the Pyr ring. Considering the structure of $(G^{\bullet+})'$ and Tomasz's proposal,[56] the $(G^{\bullet+})'$ may act as a precursor for the formation of 8-oxo-$G^{\bullet}$ by OH addition in aqueous solutions. The results provided herein can help in understanding the oxidative DNA damage occurring in cells through the reactions with ROS.

■ ASSOCIATED CONTENT

Ⓢ Supporting Information

The Supporting Information is available free of charge on the ACS Publications website at DOI: 10.1021/acs.jpclett.5b02313.

Experimental methods including sample preparation, pulse radiolysis, and TR^3 spectroscopy combined with pulse radiolysis; the proposed structures of $G^{\bullet+}$; absorbance changes at 400 and 570 nm after pulse radiolysis of 5′-dGMP in 100 mM Na phosphate buffer (pH 7.4); and residuals of global fitting results (PDF)

■ AUTHOR INFORMATION

Corresponding Authors

*E-mail: jkchoi@ibs.re.kr.

*E-mail: majima@sanken.osaka-u.ac.jp.

Notes

The authors declare no competing financial interest.

■ ACKNOWLEDGMENTS

We thank the members of the Research Laboratory for Quantum Beam Science of ISIR, Osaka University for running the linear accelerator. This work was partly supported by a Grant-in-Aid for Scientific Research (Projects 25220806 and 25288035) from the Ministry of Education, Culture, Sports, Science and Technology (MEXT) of the Japanese Government. This work was supported by IBS-R004-G2.

■ REFERENCES

(1) Cooke, M. S.; Evans, M. D.; Dizdaroglu, M.; Lunec, J. Oxidative DNA damage: Mechanisms, mutation, and disease. *FASEB J.* **2003**, *17*, 1195−1214.

(2) O'Neill, P.; Chapman, P. W. Potential repair of free-radical adducts of dGMP and dG by a series of reductants. A pulse radiolytic study. *Int. J. Radiat. Biol.* **1985**, *47*, 71−80.

(3) Teoule, R. Radiation-induced DNA damage and its repair. *Int. J. Radiat. Biol.* **1987**, *51*, 573−589.

(4) Vieira, A. J. S. C.; Steenken, S. Pattern of hydroxyl radical reaction with adenine and its nucleosides and nucleotides. Characterization of 2 types of isomeric hydroxy adduct and their unimolecular transformation reactions. *J. Am. Chem. Soc.* **1990**, *112*, 6986−6994.

(5) Dizdaroglu, M. Oxidative damage to DNA in mammalian chromatin. *Mutat. Res., DNAging: Genet. Instab. Aging* **1992**, *275*, 331−342.

(6) Dizdaroglu, M.; Laval, J.; Boiteux, S. Substrate specificity of the Escherichia coli endonuclease III: Excision of thymine- and cytosine-derived lesions in DNA produced by radiation-generated free radicals. *Biochemistry* **1993**, *32*, 12105−12111.

(7) Breen, A. P.; Murphy, J. A. Reactions of oxyl radicals with DNA. *Free Radical Biol. Med.* **1995**, *18*, 1033−1077.

(8) Dizdaroglu, M.; Jaruga, P.; Birincioglu, M.; Rodriguez, H. Free radical-induced damage to DNA: Mechanisms and measurement. *Free Radical Biol. Med.* **2002**, *32*, 1102−1115.

(9) Goodsell, D. S. The molecular perspective: Ultraviolet light and pyrimidine dimers. *Oncologist* **2001**, *6*, 298−299.

(10) Whitmore, S. E.; Potten, C. S.; Chadwick, C. A.; Strickland, P. T.; Morison, W. L. Effect of photoreactivating light on UV radiation-induced alterations in human skin. *Photodermatol., Photoimmunol. Photomed.* **2001**, *17*, 213−217.

(11) Kim, S. T.; Malhotra, K.; Smith, C. A.; Taylor, J. S.; Sancar, A. Characterization of (6−4) photoproduct DNA photolyase. *J. Biol. Chem.* **1994**, *269*, 8535−8540.

(12) Zhao, X.; Liu, J.; Hsu, D. S.; Zhao, S.; Taylor, J. S.; Sancar, A. Reaction mechanism of (6−4) photolyase. *J. Biol. Chem.* **1997**, *272*, 32580−32590.

(13) Hitomi, K.; Nakamura, H.; Kim, S. T.; Mizukoshi, T.; Ishikawa, T.; Iwai, S.; Todo, T. Role of two histidines in the (6−4) photolyase reaction. *J. Biol. Chem.* **2001**, *276*, 10103−10109.

(14) Essen, L. O.; Klar, T. Light-driven DNA repair by photolyases. *Cell. Mol. Life Sci.* **2006**, *63*, 1266−1277.

(15) Saito, I.; Takayama, M.; Sugiyama, H.; Nakatani, K.; Tsuchida, A.; Yamamoto, M. Photoinduced DNA cleavage via electron transfer: Demonstration That guanine residues located 5′ to guanine are the most electron-donating sites. *J. Am. Chem. Soc.* **1995**, *117*, 6406−6407.

(16) Sugiyama, H.; Saito, I. Theoretical studies of GC-specific photocleavage of DNA via electron transfer: Significant lowering of ionization potential and 5′-localization of HOMO of stacked GG bases in B-form DNA. *J. Am. Chem. Soc.* **1996**, *118*, 7063−7068.

(17) Prat, F.; Houk, K. N.; Foote, C. S. Effect of guanine stacking on the oxidation of 8-oxoguanine in B-DNA. *J. Am. Chem. Soc.* **1998**, *120*, 845−846.

(18) Yoshioka, Y.; Kitagawa, Y.; Takano, Y.; Yamaguchi, K.; Nakamura, T.; Saito, I. Experimental and theoretical studies on the selectivity of GGG triplets toward one-electron oxidation in B-form DNA. *J. Am. Chem. Soc.* **1999**, *121*, 8712−8719.

(19) Rakvin, B.; Herak, J. N.; Voit, K.; Huttermann, J. Free radicals from single crystals of deoxyguanosine 5′-monophosphate (Na salt) irradiated at low temperatures. *Radiat. Environ. Biophys.* **1987**, *26*, 1−12.

(20) Kobayashi, K.; Tagawa, S. Direct observation of guanine radical cation deprotonation in duplex DNA using pulse radiolysis. *J. Am. Chem. Soc.* **2003**, *125*, 10213−10218.

(21) Ribaut, C.; Bordeau, G.; Perio, P.; Reybier, K.; Sartor, V.; Reynes, O.; Fabre, P. L.; Chouini-Lalanne, N. EPR spectroelectrochemical investigation of guanine radical formation and environment effects. *J. Phys. Chem. B* **2014**, *118*, 2360−2365.

DOI: 10.1021/acs.jpclett.5b02313
J. Phys. Chem. Lett. 2015, 6, 5045−5050

(22) Candeias, L. P.; Steenken, S. Ionization of purine nucleosides and nucleotides and their components by 193-nm laser photolysis in aqueous solution: Model studies for oxidative damage of DNA. *J. Am. Chem. Soc.* **1992**, *114*, 699−704.
(23) Reynisson, J.; Steenken, S. DNA-base radicals. Their base pairing abilities as calculated by DFT. *Phys. Chem. Chem. Phys.* **2002**, *4*, 5346−5352.
(24) Rokhlenko, Y.; Cadet, J.; Geacintov, N. E.; Shafirovich, V. Mechanistic aspects of hydration of guanine radical cations in DNA. *J. Am. Chem. Soc.* **2014**, *136*, 5956−5962.
(25) Reynisson, J.; Steenken, S. DFT calculations on the electrophilic reaction with water of the guanine and adenine radical cations. A model for the situation in DNA. *Phys. Chem. Chem. Phys.* **2002**, *4*, 527−532.
(26) Kumar, A.; Sevilla, M. D. Influence of hydration on proton transfer in the guanine-cytosine radical cation ($G^{\bullet+}$-C) base pair: A density functional theory study. *J. Phys. Chem. B* **2009**, *113*, 11359−11361.
(27) Rokhlenko, Y.; Geacintov, N. E.; Shafirovich, V. Lifetimes and reaction pathways of guanine radical cations and neutral guanine radicals in an oligonucleotide in aqueous solutions. *J. Am. Chem. Soc.* **2012**, *134*, 4955−4962.
(28) Adhikary, A.; Malkhasian, A. Y.; Collins, S.; Koppen, J.; Becker, D.; Sevilla, M. D. UVA-visible photo-excitation of guanine radical cations produces sugar radicals in DNA and model structures. *Nucleic Acids Res.* **2005**, *33*, 5553−5564.
(29) Kumar, A.; Sevilla, M. D. Sugar radical formation by a proton coupled hole transfer in 2′-deoxyguanosine radical cation (2′-$dG^{\bullet+}$): A theoretical treatment. *J. Phys. Chem. B* **2009**, *113*, 13374−13380.
(30) Adhikary, A.; Collins, S.; Khanduri, D.; Sevilla, M. D. Sugar radicals formed by photoexcitation of guanine cation radical in oligonucleotides. *J. Phys. Chem. B* **2007**, *111*, 7415−7421.
(31) Gervasio, F. L.; Laio, A.; Iannuzzi, M.; Parrinello, M. Influence of DNA structure on the reactivity of the guanine radical cation. *Chem. - Eur. J.* **2004**, *10*, 4846−4852.
(32) Dimitrijevic, N. M.; Bartels, D. M.; Jonah, C. D.; Takahashi, K.; Rajh, T. Radiolytically induced formation and optical absorption spectra of colloidal silver nanoparticles in supercritical ethane. *J. Phys. Chem. B* **2001**, *105*, 954−959.
(33) Fujitsuka, M.; Majima, T. Recent approach in radiation chemistry toward material and biological science. *J. Phys. Chem. Lett.* **2011**, *2*, 2965−2971.
(34) Choi, J.; Fujitsuka, M.; Tojo, S.; Majima, T. Folding dynamics of cytochrome *c* using pulse radiolysis. *J. Am. Chem. Soc.* **2012**, *134*, 13430−13435.
(35) Thomas, M. F.; Li, L. L.; Handley-Pendleton, J. M.; van der Lelie, D.; Dunn, J. J.; Wishart, J. F. Enzyme activity in dialkyl phosphate ionic liquids. *Bioresour. Technol.* **2011**, *102*, 11200−11203.
(36) Skotnicki, K.; Bobrowski, K. Molecular hydrogen formation during water radiolysis in the presence of zirconium dioxide. *J. Radioanal. Nucl. Chem.* **2015**, *304*, 473−480.
(37) Balcerzyk, A.; Schmidhammer, U.; Horne, G.; Wang, F. R.; Ma, J.; Pimblott, S. M.; de la Lande, A.; Mostafavi, M. Unexpected ultrafast silver ion reduction: Dynamics driven by the solvent structure. *J. Phys. Chem. B* **2015**, *119*, 10096−10101.
(38) Fujitsuka, M.; Cho, D. W.; Tojo, S.; Choi, J.; Huang, H.-H.; Yang, J.-S.; Majima, T. Radical cation of star-shaped condensed oligofluorenes having isotruxene as a core: Importance of rigid planar structure on charge delocalization. *J. Phys. Chem. A* **2014**, *118*, 2307−2315.
(39) Choi, J.; Cho, D. W.; Tojo, S.; Fujitsuka, M.; Majima, T. Configurational changes of heme followed by cytochrome c folding reaction. *Mol. BioSyst.* **2015**, *11*, 218−222.
(40) Choi, J.; Cho, D. W.; Tojo, S.; Fujitsuka, M.; Majima, T. Structural study of various substituted biphenyls and their radical anions based on time-resolved resonance Raman spectroscopy combined with pulse radiolysis. *J. Phys. Chem. A* **2015**, *119*, 851−856.
(41) Candeias, L. P.; Steenken, S. Structure and acid-base properties of one-electron-oxidized deoxyguanosine, guanosine, and 1-methylguanosine. *J. Am. Chem. Soc.* **1989**, *111*, 1094−1099.
(42) Candeias, L. P.; Steenken, S. Electron-transfer in di(deoxy)-nucleoside phosphates in aqueous solution: Rapid migration of oxidative damage (via adenine) to guanine. *J. Am. Chem. Soc.* **1993**, *115*, 2437−2440.
(43) Stemp, E. D. A.; Arkin, M. R.; Barton, J. K. Oxidation of guanine in DNA by $Ru(phen)_2(dppz)^{3+}$ using the flash-quench technique. *J. Am. Chem. Soc.* **1997**, *119*, 2921−2925.
(44) Wu, L. D.; Liu, K. H.; Jie, J. L.; Song, D.; Su, H. M. Direct observation of guanine radical cation deprotonation in G-quadruplex DNA. *J. Am. Chem. Soc.* **2015**, *137*, 259−266.
(45) Choi, J.; Park, J.; Tanaka, A.; Park, M. J.; Jang, Y. J.; Fujitsuka, M.; Kim, S. K.; Majima, T. Hole trapping of G-quartets in a G-quadruplex. *Angew. Chem., Int. Ed.* **2013**, *52*, 1134−1138.
(46) Toyama, A.; Hanada, N.; Ono, J.; Yoshimitsu, E.; Takeuchi, H. Assignments of guanosine UV resonance Raman bands on the basis of ^{13}C, ^{15}N and ^{18}O substitution effects. *J. Raman Spectrosc.* **1999**, *30*, 623−630.
(47) Fodor, S. P. A.; Rava, R. P.; Hays, T. R.; Spiro, T. G. Ultraviolet resonance raman-spectroscopy of the nucleotides with 266-nm, 240-nm, 218-nm, and 200-nm pulsed laser excitation. *J. Am. Chem. Soc.* **1985**, *107*, 1520−1529.
(48) Beck, S. M.; Brus, L. E. The resonance Raman-spectra of queous phenoxy and phenoxy-D_5 radicals. *J. Chem. Phys.* **1982**, *76*, 4700−4704.
(49) Mukherjee, A.; Mcglashen, M. L.; Spiro, T. G. Ultraviolet resonance Raman-spectroscopy and general valence force-field analysis of phenolate and phenoxyl radical. *J. Phys. Chem.* **1995**, *99*, 4912−4917.
(50) Tripathi, G. N. R.; Schuler, R. H. The Time-resolved resonance Raman-spectrum of pulse radiolytically produced phenoxyl radical. *Chem. Phys. Lett.* **1983**, *98*, 594−596.
(51) Tripathi, G. N. R.; Schuler, R. H. The resonance Raman-spectrum of phenoxyl radical. *J. Chem. Phys.* **1984**, *81*, 113−121.
(52) Tripathi, G. N. R.; Schuler, R. H. Resonance Raman studies of pulse radiolytically produced *p*-aminophenoxyl radical. *J. Phys. Chem.* **1984**, *88*, 1706−1710.
(53) Giese, B.; McNaughton, D. Density functional theoretical (DFT) and surface-enhanced Raman spectroscopic study of guanine and its alkylated derivatives: Part 1. DFT calculations on neutral, protonated and deprotonated guanine. *Phys. Chem. Chem. Phys.* **2002**, *4*, 5161−5170.
(54) Greco, F.; Liguori, A.; Sindona, G.; Uccella, N. Gas-phase proton affinity of deoxyribonucleosides and related nucleobases by fast-atom-bombardment tandem mass-spectrometry. *J. Am. Chem. Soc.* **1990**, *112*, 9092−9096.
(55) Steenken, S. Purine-bases, nucleosides, and nucleotides: Aqueous solution redox chemistry and transformation reactions of their radical cations and e^- and OH adducts. *Chem. Rev.* **1989**, *89*, 503−520.
(56) Tomasz, M.; Olson, J.; Mercado, C. M. Mechanism of the isotopic exchange of the C-8 hydrogen of purines in nucleosides and in deoxyribonucleic acid. *Biochemistry* **1972**, *11*, 1235−1241.

DOI: 10.1021/acs.jpclett.5b02313
J. Phys. Chem. Lett. 2015, 6, 5045−5050